Unlocking high-performance hydrogen evolution: Argon-induced Ni segregation in NiO/TiO2 of core/shell catalysts

Hassan E Gomaa, Heba H El-Maghrabi, Fatma A Gomaa, Patrice Raynaud, Amr A Nada

Unlocking High-Performance Hydrogen Evolution: Argon-Induced Ni Segregation in NiO/TiO_2 of Core/Shell Catalysts

Hassan E. Gomaa[1,2,3], Heba H. El-Maghrabi[4,5,*], Fatma A. Gomaa[1,6], Patrice Raynaud[5], Amr A. Nada[5,7,*]

[1]Department of Chemistry, College of Science and Humanities, Shaqra University, Ad-Dawadmi 11911, Saudi Arabia.
[2]Department of Nuclear Safety Engineering, Nuclear Installations Safety Division, Atomic Energy Authority, 11765, Egypt
[3]Water Research Group, College of Science and Humanities at Ad-Dawadmi, Shaqra University, Ad-Dawadmi 11911, Saudi Arabia
[4]Refining Department, Egyptian Petroleum Research Institute (EPRI), Cairo 11727, Egypt
[5]Laboratoire Plasma et Conversion d'Energie (LAPLACE), Université de Toulouse, CNRS, INPT, UPS, 31062, Toulouse, France
[6]Department of Chemistry, College of Women for Science, Arts, and Education, Ain Shams University, 11757, Egypt
7Department of Analysis and Evaluation, Egyptian Petroleum Research Institute, Cairo, 11727, Egypt
* hebachem@yahoo.com (H.H.E.) amr.nada@umontpellier.fr (A.A.N.)

ABSTRACT

This study introduces novel core-shell structured electrocatalysts synthesized via an optimized one-pot sol-gel method, aimed at enhancing the efficiency of the Hydrogen Evolution Reaction (HER) in water splitting. The Ni-NiO/TiO_2 and NiO/TiO_2 composites demonstrate superior catalytic performance, with the Ni-NiO/TiO_2 requiring a remarkably low potential of -0.125 V versus Ag/AgCl to achieve a current density of 10 mA.cm-². This performance surpasses that of NiO/TiO_2 and pure NiO, offering a viable alternative to Pt catalysts. Advanced characterization techniques, including X-ray diffraction, electron microscopy, and X-ray photoelectron spectroscopy, elucidate the crystalline phases, morphologies, and chemical states, enhancing our understanding of the electrocatalysts' efficiency. In particular, Rietveld refinement analysis provides detailed insights into the structural properties that underpin the observed catalytic performance. Electrochemical assessments highlighted the Ni-NiO/TiO_2 composite's reduced overpotential needs, high Faradaic efficiency (~98%), and notable long-term durability, positioning these materials as promising candidates for sustainable hydrogen production.

Keywords: Hydrogen Production, Water Splitting, Core-Shell Electrocatalysts, Ni-NiO/TiO_2 Composites, Argon-Induced Segregation, Sustainable Energy Solutions

Introduction

There is a growing awareness that hydrogen fuel stands out as an up-and-coming replacement for fossil fuels in future energy scenarios [1]–[5]. Its eco-friendliness and renewability are among the notable advantages where hydrogen can be sustainably derived through electrolytic water splitting, known as the hydrogen evolution reaction (HER) [6]–[10]. Electrocatalysis is crucial in the HER process, especially the electrocatalyst fabrication [11], since up to now, Pt group metals (Pd, Pt, and Ru) have demonstrated the most efficient electrocatalysts thanks to their effective charge carrier separation [12], [13]. However, the practical limitations of scarcity and high costs associated with Pt group metals have hindered their widespread use in commercial hydrogen production processes [14]–[16]. As a result, the quest for efficient Pt-free HER catalysts has become a global research objective, particularly those derived from cost-effective and widely available materials [17], [18]. One commonly explored approach involves synthesizing a metals-semiconductor Schottky heterojunction [19]–[22]. Within this context, the formation of an n-p junction by combining an electron-rich (n-type) semiconductor with a hole-rich a (p-type) one proves to be a successful strategy for efficiently separating simultaneously generated electrons and holes driven by the built-in electric field, thereby enhancing catalytic performance [23]–[25].

The earth-abundant nickel oxide (NiO) proposed and used as a p-type semiconductor with titanium dioxide (TiO_2) as an n-type to form an n-p heterojunction for efficient electron-hole separation has recently gained researchers' attention [26], [27]. Various fabrication methods have been devised and implemented to successfully synthesise nanocomposites of TiO_2-NiO for catalytic applications, including hydrothermal [28]–[30], incipient wetness impregnation [31], [32], solvothermal [33]–[35], sol–gel [36], [37], ultrasonication [38], [39], and evaporation-induced methods [40]. Among all the various developed methods, the sol-gel method is widely used in industrial applications for generating significant quantities of nanomaterials compared to other approaches [41] thanks to its unique properties for consistently producing high-quality nanoparticles on an industrial scale [42].

The sol-gel method has the merits of efficient and cost-effective synthesizing nanoparticle composites of two or more metals in a single step with diverse chemical compositions by blending specific proportions of the metals' precursors [43]–[45]. Despite the enhanced charge carrier separation facilitated by the built-in electric field, the commonly synthesised nanocomposites possess defects in the established n-p heterojunction interfaces, leading to reduced catalytic efficiency due to the induced rapid charge recombination. Suppressing such charge carrier

recombination could be attained through an intermediate medium for charge transfer at the interface. However, challenges remain significant in synthesizing such a sophisticated structure and optimising its performance. Therefore, there is a need to develop facile and scalable methods to fabricate nanocomposites with architectures facilitating rapid charge transfer, enhancing the catalytic performance of this n-p heterojunction system [46]–[52].

While Ni-based nanomaterials exhibit favourable electrocatalytic properties, there has been limited exploration in recent studies regarding their application as platinum (Pt) alternative electrocatalysts for the HERs. For instance, electrospun C@NiO/Ni nanofibers obtained through a subsequent carbonisation process demonstrated notable electrocatalytic efficiency for HER, maintaining effectiveness and stability for up to 22 hours [53]. Double surface-decorated Ni nanofibers of NiO and CrO_3 (Ni@ NiO@CrO_3) were developed, giving electrocatalytic activity of 100 mA cm^{-2} at a low overpotential of 228 mV versus the reversible hydrogen electrode (RHE) with superior stability as it lasted, without decay, over 120 hours [54]. Yan et al. reported on Ni/NiO nanosheets of crystalline/amorphous core/shell in structure, which yielded, with sustained stability, an HER current density of 5 $mAcm^{-2}$ at 110 mV overpotential [55]. El-maghrabi et al. presented coaxial nickel/gadolinium oxide/nickel oxide nanofibers, which proved an exceptionally efficient electrocatalyst for HER. This configuration demonstrated an impressively low onset potential of approximately 32 mV, coupled with remarkable long-term durability evidenced by the successful completion of 5000 cycles [56]. To merge NiO with an (n-type) semiconductor like TiO_2, researchers such as Chen et al. elucidated the remarkable catalytic prowess of NiO/TiO_2 in the degradation of methylene blue. This effectiveness was attributed to the forming of a p-n junction, coupled with the co-catalyst effect of TiO_2 and NiO. The introduction of metallic nickel to the heterostructure (NiO-TiO_2) has the potential to improve charge separation during water splitting, consequently enhancing the overall activity for hydrogen production. For instance, Yu and collaborators detailed the synthesis of a Ni-$Ni(OH)_2$-TiO_2 nanocomposite [57], while El-maghrabi and colleagues employed plasma-enhanced chemical vapour deposition (PECVD) to fabricate nanocomposites of Ni/NiO-TiO_2/rGO onto carbon cloth, demonstrating their efficacy for hydrogen production [19]. The heterostructure configuration emerged as a critical factor influencing its catalytic utility. Yin and collaborators highlighted the significance of core-shell nanostructured electrocatalysts in altering water-splitting dynamics. They emphasised the importance of modifying electronic interactions between cores and shells to achieve enhanced interfacial

synergy, consequently reinforcing long-term durability, particularly in corrosive electrolytes under the protective influence of robust shells. An organisational categorisation based on core components, such as transition metals (TMs), transition metal oxides (TM(H)Os), transition metal phosphides (TMPs), transition metal carbides (TMCs), and transition metal dichalcogenides (TMDs) was proposed [58]. Consisting of a core (inner material) and a shell (outer layer material), electrocatalysts with a core-shell architecture have the potential to enhance both efficiency and long-term durability during water splitting. Notably, core-shell nanostructures featuring minimal amounts of noble metals in their thin shells contribute to cost reduction while facilitating robust interactions between the core components and noble metals [59]–[61]. This interaction, in turn, imparts high activity and stability to the composite material.

The manipulation of core-shell nanostructures is crucial for generating extensively exposed active surfaces, systematically adjusting the chemical and electronic configurations of interfacial sites, achieving synergistic enhancements across multiple sites through the cores and shells and enhancing the long-term durability, particularly in corrosive media, with the safeguard of robust shells. In our study, we aim to design and successfully construct an n-p heterojunction of NiO/TiO_2 with an ultrafine structure of core-shell arrangement through a facile one-pot method in the presence of Ni^0 on the surface, emphasizing the structural characteristics of core-shell materials and their advantages for electrocatalysis. The nano-interfaces within the NiO/TiO_2 heterostructure are anticipated to augment the HER by providing stability to hydrogen atoms on metallic Ni, thereby releasing the produced OH^- on NiO/TiO_2. Additionally, zero-valent Ni on the surface of NiO/TiO_2 might facilitate the transfer of electrons. However, it is observed that NiO/Ni heterostructures are inherently unstable and experience significant degradation over time. Building upon the insight that the core-shell structure of Ni-based materials can enhance corrosion resistance and stability [62], a NiO/TiO_2 core-shell design is adopted and implemented to foster the heterostructure stability of Ni/NiO.

Furthermore, the TiO_2 and NiO interaction is anticipated to create new catalytic sites by forming a p-n junction at the interfaces. The synthesised electrocatalyst demonstrates exceptional performance in the HER, boasting an onset potential of 88 mV, nearly indistinguishable from platinum's performance. Additionally, the presence of nickel in the NiO/TiO_2 structure contributes to its long-term durability, which is evident after an accelerated scan of 1000 cycles. Furthermore,

the facile integration of Ni at NiO/TiO_2 into HER electrolysers surpasses benchmark Pt catalysts' performance.

In this study, we explore the innovative approach of electronic modulation through doping in the design of advanced electrocatalysts for the Hydrogen Evolution Reaction (HER). By introducing nickel into the TiO_2 matrix to create $Ni\text{-}NiO/TiO_2$ composites, we aim to harness the electronic interactions that significantly enhance the catalytic activity. Doping with nickel not only alters the electronic properties of TiO_2 but also optimizes the charge transfer processes crucial for effective catalysis. This strategic incorporation of nickel leads to improved electronic conductivity and facilitates a more efficient separation and transfer of charge carriers at the catalytic sites. The novelty of our approach lies in the tailored manipulation of the electronic environment within the catalyst structure, which is theorized to reduce overpotential and increase the HER activity, offering a substantial improvement over traditional noble metal catalysts. This method stands out as it provides a detailed understanding of how elemental doping can be used to fine-tune material properties for specific catalytic roles, paving the way for the development of cost-effective, high-performance electrocatalysts tailored for sustainable energy applications.

2. Experimental

2.1 Materials and chemicals

All reagents employed, ethanol, tetraisopropyl titanate ($Ti(OC_3H_7)_4$) TTIP, nickel nitrate ($Ni(NO_3)_2.6H_2O$), and sodium hydroxide (NaOH), readily available commercially and procured from Sigma Aldrich, were of analytical grade and used without further purification.

2.2 Experimental Procedure

Nickel nitrate, serving as the Ni precursor, was used to synthesize solid NiO through a sol-gel method. Initially, 0.489 g of nickel nitrate was dissolved in 50 ml of ethanol. Subsequently, 2 ml of 1 M NaOH solution was added dropwise with continuous stirring. Following this, a syringe pump injected a mixture of 1 mL of tetraisopropyl titanate (TTIP) and 5 mL of absolute ethanol at a rate of 0.5 mL/minute. The mixture was then stirred at 900 rpm and heated to 85 °C with refluxing for 90 minutes, resulting in a milk-like gel. Using a steam-modified sol-gel technique, water vapor was gradually introduced for 2 hours using a humidifier. The resulting NiO/TiO_2 precipitate was centrifuged and rinsed three times with ethanol. The separated solids were then dried and calcined at 400 °C with a heating rate of 1 °C/min for 3 hours under different atmospheres (air for NiO/TiO_2

and argon for Ni/NiO/TiO_2) to produce core-shell nanoparticles, respectively. The same procedure was applied to prepare pure NiO nanoparticles, with the exception of omitting the TTIP.

2.3 Characterisation

The fabricated electrocatalyst's crystalline phases were investigated using a PANalytical Xpert-PRO X-ray diffractometer instrumented with an Xcelerator detector with Ni-filtered Cu radiation source λ equal to 1.54 Å. The samples' morphology and structure were investigated using a Hitachi S4800, Japan, scanning electron microscopy (SEM) and a JEOL JEM 2100, JEOL, Japan, transmission electron microscopy (TEM). These examinations were conducted at 200 kV accelerating voltage, and the system was equipped with energy-dispersive X-ray (EDX) spectroscopy for detailed compositional analysis. The Escalab 250, Thermo Fisher Scientific, USA, XPS machine (X-ray Photoelectron Spectroscopy) was employed to conduct the XPS analysis utilizing the monochromatic radiation of AlKα (1486.6 eV) at settings of 1 µA and 2 kV. The analysis encompassed 400 µm surface diameter, and data acquisition was carried out for 1203.5 seconds to determine the elemental composition.

2.4 The Electrochemical Tests

A Solartron SI 1287 galvanostatic-potentiostat was employed to carry out the electrochemical tests. The setup was in a three-electrode configuration, including an Ag/AgCl reference electrode, platinum counter-electrode, and the working electrode prepared with the fabricated catalyst. The working electrode was prepared by depositing and drying 20 µL of the uniform electrocatalyst ink onto a 3 mm diameter glassy carbon electrode. The uniform catalyst ink was prepared by sonicating for 15 minutes a blend of 5 mg of the prepared electrocatalysts, 40 µL NAFION solution, and 1 mL isopropanol alcohol. The three electrodes were immersed in an electrolyte solution of 0.5 M H_2SO_4, yielding a potential of 0.197 V vs. RHE at room temperature. A standard material consisting of a Pt wire obtained from CH-instrument, USA, was used for comparison on the cathode side. The linear sweep voltammetry (LSV) technique was used to evaluate the HER at 5 mV/s scan rate, and the cyclic voltammograms (CV) were obtained in the 0.1 V - 0.3 V potential range at varying scan rates from 10 to 100 mV/s. Moreover, the electrochemical impedance spectroscopy (EIS) was carried out over a 0.1 Hz to 1 MHz frequency range at 0.2 V vs. RHE with a ten mV voltage bias. All electrochemical tests were conducted at ambient temperature and

pressure conditions. The Clarus-400, PerkinElmer, gas chromatograph equipped with a TCD of 2 m x 1 mm employing He as the carrier gas was used to quantify the hydrogen gas produced.

3. Results and Discussion

3.1 Characterisation Results of the Fabricated Catalysts

Composites consisting of NiO, NiO/TiO2, and Ni-NiO/TiO2 with a core-shell structure were successfully developed, explicitly targeting the enhancement of hydrogen production efficiency.

The cubic NiO phase was identified in the XRD pattern recorded for NiO with no extra peaks detected, demarcating the purity of the fabricated electrocatalysts belonging to the Fm-3m space group of the JCPDS card no. 01-75-0269, as shown in Figure 1a. Meanwhile, the crystalline TiO_2 phase XRD patterns were identified in the NiO/TiO_2 (match of the JCPDS card 01-084-1285) and the Ni-NiO/TiO_2 samples, revealing the crystalline nature of the TiO_2 shell on the NiO core with patterns representative of Ni metal according to the reference structures PDF #004-0850. Such patterns confirm a crystalline metallic zero-valent Ni phase formation during the heat treatment under Ar for the NiO/TiO_2 sample, agreeing with the previous studies [62]. A nanocrystalline NiO phase with a mean size of 44.3 ± 0.5 nm and a minor microstrain of 1.43 was estimated using the Rietveld refinement analysis using Fullprof. The cubic NiO phase lattice parameter, a, was evaluated as 4.1777 Å, comparable to the value reported in [63].

The metallic Ni phase was observed to segregate, 3.1 wt%, upon calcination under the Ar atmosphere of the Ni-NiO/TiO_2 sample with a decrease in the NiO phase share. Moreover, the cubic NiO lattice parameters of the NiO/TiO_2 were quite the same as the pure NiO, indicating that no secondary phase of $NiTiO_3$ phases formed when calcined under an air atmosphere. The calculated parameters through Rietveld refinement analysis, including lattice parameters, crystallite size, and weight fractions, are summarised in Table 1. The inspection of such data in Table 1 indicates that NiO phase crystallite size was reduced when combined with the TiO_2 phase, which agrees with SEM findings shown in Figure 2. Moreover, in the Ni-NiO/TiO_2 sample, the NiO phase exhibited a lower microstrain value compared to that in the case of the NiO/TiO_2 sample and decreased in lattice parameter, which might result from the segregation of Ni from the NiO lattice when annealed under an Ar atmosphere [62].

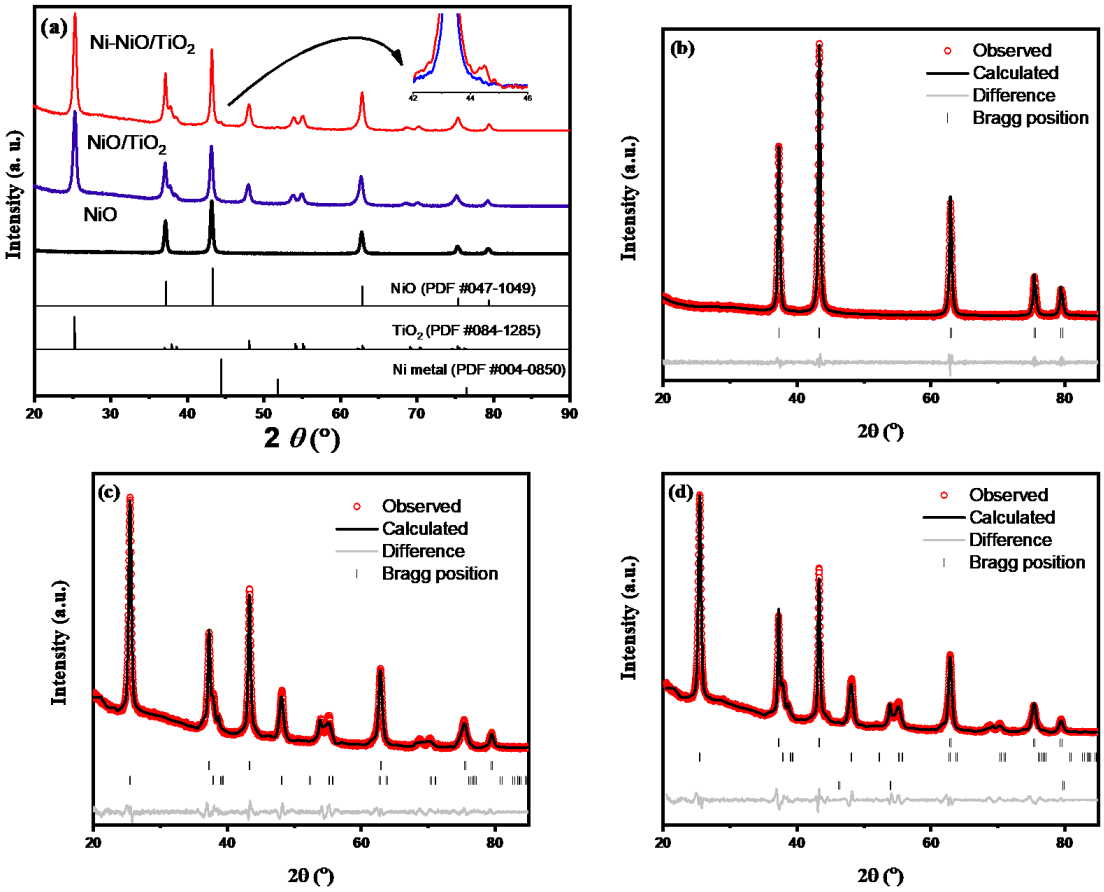

Figure 1: **X-ray patterns and their processed spectra of the produced catalysts.** a. XRD spectra of the fabricated catalysts, b. Rietveld refined spectra of the NiO sample, c. Rietveld refined spectra of the NiO/TiO_2 sample, and d. Rietveld refined spectra of the $Ni\text{-}NiO/TiO_2$ sample.

Table 1: Summary of the Rietveld refinement extracted structural parameters from powder XRD spectra of NiO, NiO/TiO_2, and $Ni^o\text{-}NiO/TiO_2$ nanofibers.

Sample Name	**NiO phase**				**TiO_2**		**Ni^o metal**	
	Lattice parameter, Å	Mass fraction, %	Crystal Size, nm	Microstrain $x10^{-4}$	Mass fraction, %	Crystal size, nm	Mass fraction, %	Crystal size, nm
NiO	4.1777(3)	100	44.3(5)	1.43	-	-	-	-
NiO/TiO_2	4.1762(2)	84.3(4)	42.7(2)	1.64	15.5(6)	12.3(2)	-	-
Ni- NiO/TiO_2	4.1721(1)	81.1(5)	40.2(4)	1.32	15.3(3)	11.7(2)	3.1(3)	6.8(7)

SEM, TEM, and HRTEM were employed to investigate the morphologies of NiO, NiO/TiO_2, and Ni-NiO/TiO_2 samples, as depicted in Figure 2a. SEM imagery reveals that NiO primarily consists of large quasi-spherical and spherical particles, with an average size of approximately 55 ± 8 nm. The incorporation of TiO_2 did not alter the morphology of NiO, as evidenced in Figures 2b and 2c. The TEM image of the Ni-NiO/TiO_2 sample, shown in Figure 2d, displays a conformal layer encasing the NiO nanoparticles, identified as the TiO_2 shell. Energy Dispersive X-ray (EDX) analysis confirms the presence of a mesoporous NiO core enveloped by a thin TiO_2 shell. The HRTEM image in Figure 2e shows that the NiO nanoparticles exhibit clear and well-defined lattice fringes, indicating a high degree of crystallinity. The average fringe spacing measured at 2.41±0.06 Å aligns with the (111) plane distances typically found in the NiO phase, which forms the core. Similarly, the fringe spacing of 3.52±0.05 Å matches the (101) crystallographic plane of the anatase structure, indicating its presence as the shell.

Furthermore, EDX elemental mapping, illustrated in Figure 2f-h, demonstrates the uniform distribution of Ti (Figure 2g) on the surface of Ni elements (Figure 2f) within the Ni-NiO/TiO_2 sample. However, TiO_2 predominantly appears on the surface of the NiO core in the Ni-NiO/TiO_2 sample, with some Ni also segregated on the surface. This segregation of metallic Ni phases follows calcination in an argon atmosphere, as discussed in our previous work [64].

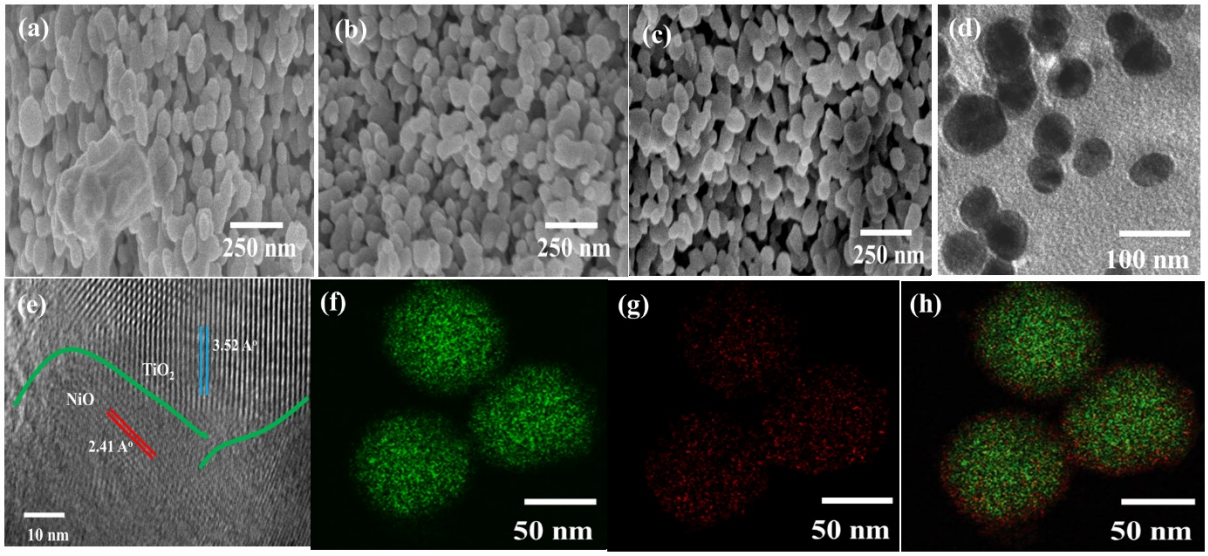

Figure 2: presents field-emission SEM, TEM, and EDX analyses of the fabricated materials. It includes SEM images of NiO (a), NiO/TiO_2 (b), and Ni-NiO/TiO_2 (c). The TEM image of Ni-

NiO/TiO_2 (d), HRTEM of Ni-NiO/TiO_2 (e), The EDX elemental mapping, which illustrates the distribution of Ni element (f), the Ti element (g), and the overlap of Ni and Ti elements (h).

The oxidation states and chemical compositions of constituting elements on the surfaces were investigated employing XPS. High-resolution XPS spectra of Ni 2p, Ti 2p, and O 1S orbitals are illustrated in Figures 3(a-c). In Figure 3a, the $2p_{3/2}$ spectra of Ni in the NiO and NiO/TiO_2 samples show two distinct peaks at 854 and 855.5 eV, accompanied by a broad satellite peak at 861 eV. These findings closely match the peak positions previously reported for NiO [56], [65].
In contrast, the XPS peaks of the Ni-NiO/TiO_2 sample have shifted to lower binding energies by ~ 0.53 eV, indicating a reduction in the oxidation state of the nickel cations. This is corroborated by the presence of metallic Ni, as identified by XRD in Figure 1 [66], [67]. In Figure 3b, the peaks at 459.1 and 464.8 eV correspond to the $2p_{1/2}$ and $2p_{3/2}$ spectra of Ti, respectively, in both the NiO/TiO_2 and Ni-NiO/TiO_2 samples. These results are consistent with previously reported data for TiO_2 [68]. In the Ni-NiO/TiO_2 sample, the Ti 2p peak has shifted to a lower binding energy by 0.42 eV compared to the NiO/TiO_2 sample, suggesting a partial reduction of Ti^{4+} to Ti^{3+}. This shift likely causes the formation of oxygen vacancies, which enhance the catalytic properties of the material [19]. Deconvoluted peaks at ~ 529.5 and 531.5 eV are seen in Figure 3c for the O 1s spectra, which correspond to the oxygen lattice, O_{latt}, and the hydroxides, $O_{hyd,}$ respectively [69]. In the Ni-NiO/TiO_2 sample, the peak corresponding to the oxygen lattice shifted to a lower binding energy. This shift may be due to a reduction in oxygen content, resulting from oxygen removal during annealing in anoxic conditions under an argon atmosphere.

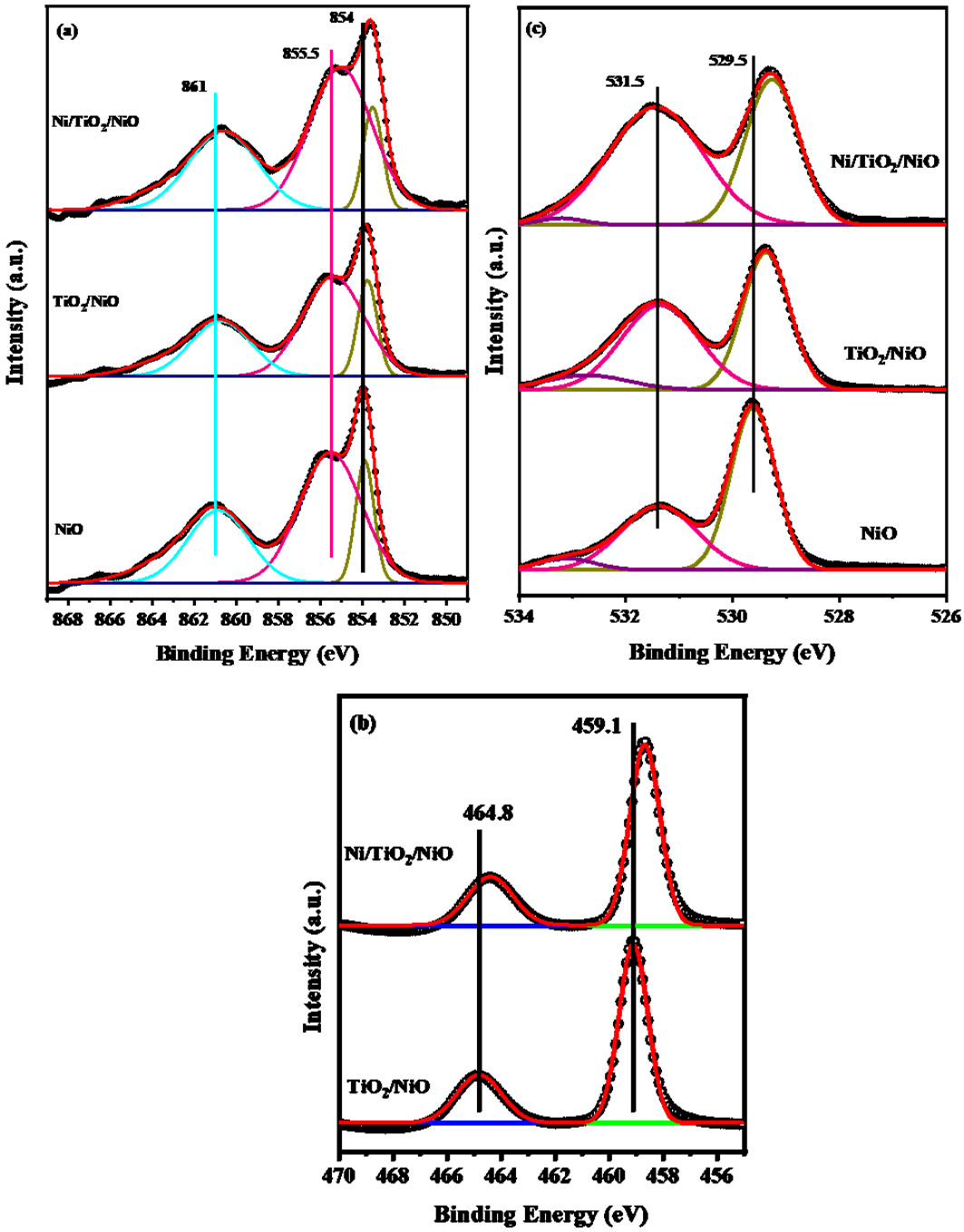

Figure 3: High-resolution XPS spectra of (a) Ni 2p, (b) Ti 2p, and (c) O 1s for NiO, NiO/TiO_2, and Ni-NiO/TiO_2 nanocomposite.

3.2 Electrochemical Tests and the Hydrogen Evolution Reaction Assessment

The catalytic performance of the prepared catalysts was experimentally assessed, and the collected data are analysed, compared, and commented on herein. Figure 4 shows the catalytic activities of the prepared catalysts concerning the HER, which generally follow the descending order Ni-NiO/TiO_2 > NiO/TiO_2 > NiO, with the pure NiO demonstrating relatively poor performance. Although TiO_2 enhances the catalytic performance by providing highly active centers for the HER when on the surface of the NiO/TiO_2, the existence of Ni in Ni-NiO/TiO_2 resulted in enhancing the Ni-NiO/TiO_2 catalyst and electrolyte solution junction, creating more active sites on the surface. Hence, the relative coverage of the core catalyst with TiO_2 and Ni on the surface of the core-shell structure is crucial for enhancing HER activity, which is corroborated by comparing the catalytic performances for Ni-NiO/TiO_2 and NiO. The pure NiO exhibited significantly lower activity than Ni-NiO/TiO_2, confirming a minimal catalytic activity in the absence of Ni and TiO_2. Moreover, Ni-NiO/TiO_2 required an overpotential of 125 mV to drive a current density of 10 $mA.cm^{-2}$, and this value is comparable to those of a series of reported research [19], [70]. The Ni-NiO/TiO_2 onset potential approached that of Pt, which may be considered an exciting industrial candidate for HER applications. On the other hand, in the process of water (H_2O) splitting, hydroxide ions (OH^-) are produced. These ions selectively bind to trivalent titanium (Ti^{3+}) sites at the material's interface. This specific attachment is driven by the potent electrostatic attraction between the negatively charged OH^- ions and the positively charged Ti^{3+} sites. Additionally, the formation of oxygen vacancies, which is a direct consequence of the presence of Ti^{3+} which is detected by XPS, further facilitates this interaction. These vacancies create an imbalance in the local charge distribution, enhancing the electrostatic attraction and leading to a more pronounced adherence of OH^- ions to that these Ti^3 sites. Finally, we conclude the superior activity of the Ni-NiO/TiO_2 sample can be attributed to three factors: (i) TiO_2 shell surround the surface of the NiO core, (ii) forming an active Ni metal through reduction under the Ar atmosphere, and (iv) a large quantity of OH^- on the catalyst surface.

A Tafel plot ($\log j$–η) was applied to appreciate the catalyst kinetics. As demonstrated in Figure 4c, via fitting with the Tafel equation ($\eta = b \log j + a$, in which η is the overpotential, j is the current density, and b is the Tafel slope), a set of slopes of 140, 57, 40 and 30 mV dec^{-1} were deliberated for the NiO, NiO/TiO_2, Ni-NiO/TiO_2 and Pt respectively. It should be distinguished that Ni-NiO/TiO_2 with a small concentration of Ni were more active in promoting the HER reaction, which is harmonious with the previous LSV results. The Tafel slope in the range of 30 to 40 mV revealed

that the HER on the Ni-NiO/TiO_2 surface follows the common Volmer–Tafel process with very high H_{ads}, with the Tafel step being the rate-determining step (RDS). The exchange current density (J_0) was calculated from the extrapolation of the Tafel plot to study the electrodes' electrochemical activity and reflect activity further. The cyclic voltammetry (CV) analysis of the fabricated samples within the potential range of +0.1 to +0.3 V, where no faradic reactions occurred, facilitated the capacitance calculation of the double layer (Figure 4d and Table 2). The double layer capacitance (C_{dl}) is proportionally with the effective electrochemical active surface area (ECSA). So, the ECSA could be calculated using the relationship ECSA = C_{dl}/Cs, where Cs equals 40 μF/cm^2, representing the atomically smooth planar surface capacitance [71]. Notably, the ECSAs of Ni-NiO/TiO_2 are 4.75 cm^2 compared to 2.52 and 0.19 cm^2 for NiO/TiO_2 and NiO, respectively. These results supported the fact that Ni-NiO/TiO_2 has the largest catalytically active sites per surface area.

Long-term durability, crucial for industrial applications, was evaluated using chronoamperometric response (Figure 4e). The results show a minimal current attenuation of only 4% after 40 hours of continuous testing at an initial overpotential of 200 mV, maintaining 96% stability over the duration. Additionally, the working electrode underwent 1000 potential cycles of continuous cyclic voltammetry (CV) measurement between 0 and −0.6 V (vs. RHE) at a scan rate of 100 mV s^{-1}. The LSV curves overlapped before and after the 1000 CV test, particularly in the low overpotential region, underscored the robust stability of the Ni-NiO/TiO_2 catalyst (Figure 4f) with $\Delta\eta$ = 10 mV. These findings confirm the superior stability of the Ni-NiO/TiO_2 catalyst for long-term HER. X-ray diffraction analysis of the Ni-NiO/TiO_2 core-shell structure after a 40-hour electrolysis test (Figure S1) indicated that the structure remained intact. Table S1 provides a straightforward comparison, underscoring the enhanced long-term stability of the Ni-NiO/TiO_2 catalyst for the hydrogen evolution reaction (HER) relative to other reported NiO systems [53], [54], [56], [66], [72]–[79].

Furthermore, Ni-NiO/TiO_2 exhibited ≈ 98%, an exceptional faradic efficiency, based on H_2 gas produced and quantified using the gas chromatography measurements during HER (Figure 4g). The superior faradic efficiency might be attributed to facilitated electron transfer in the Ni-NiO/TiO_2 sample, as explored by electrochemical impedance spectroscopy (EIS) measurements. The EISs were conducted to identify the charge transport and internal resistance of the fabricated electrocatalyst. Electrochemical impedance confers facts around the simplicity of charge

transportation on different electrode surfaces. The impedance curve was fitted with the equivalent circuit (onset of Figure 4h) consisting of the resistance R_s and R_{CT}, and the values of the resistances are summarised in Table 2. The lower charge transfer resistance of Ni-NiO/TiO_2 implies that the Ni-NiO/TiO_2 electrode offers the least resistance to electron transportation. In the acidic aqueous media, the HER unfolds in two primary stages according to the classic theory, described by the equations below:

The initial phase involves an electrochemical reduction, represented as $H_3O^+ + e^- \rightarrow H_{ads} + H_2O$. This step is known as the discharge or Volmer step and is characterised by a Tafel slope of approximately 120 mV/dec. The subsequent phase involves desorbing adsorbed hydrogen (H_ads) through two distinct mechanisms. The first mechanism is the Heyrovsky reaction, $H_{ads} + H_3O^+ + e^- \rightarrow H_2 + H_2O$, an ion-atom reaction with a Tafel slope of around 40 mV/dec. The alternative route is the Tafel reaction($H_{ads} + H_{ads} \rightarrow H_2$) a reaction between atoms with a Tafel slope of about 30 mV/dec. In this context, the electrodes being studied predominantly follow the Volmer-Tafel pathway as illustrated in Figure 5.

Furthermore, integrating NiO/TiO_2 and Ni to form an n-p junction within a single heterostructure significantly enhanced the efficiency of the Ni-NiO/TiO_2 bifunctional catalyst electrode for the HER, a crucial component of water-splitting reactions. Within this p-n junction, electrons migrate from the n-type TiO_2 to the p-type NiO, leading to the discharge through Ni. This electron movement creates negative charges, which act as active sites on the surface of Ni-NiO/TiO_2. These sites facilitate the adsorption and subsequent reduction of protons (H^+) in acidic electrolytes, thereby boosting the reaction's efficiency. All the above results reveal that the core-shell structure of the Ni-NiO/TiO_2 catalyst successfully enhances the electrochemical activity.

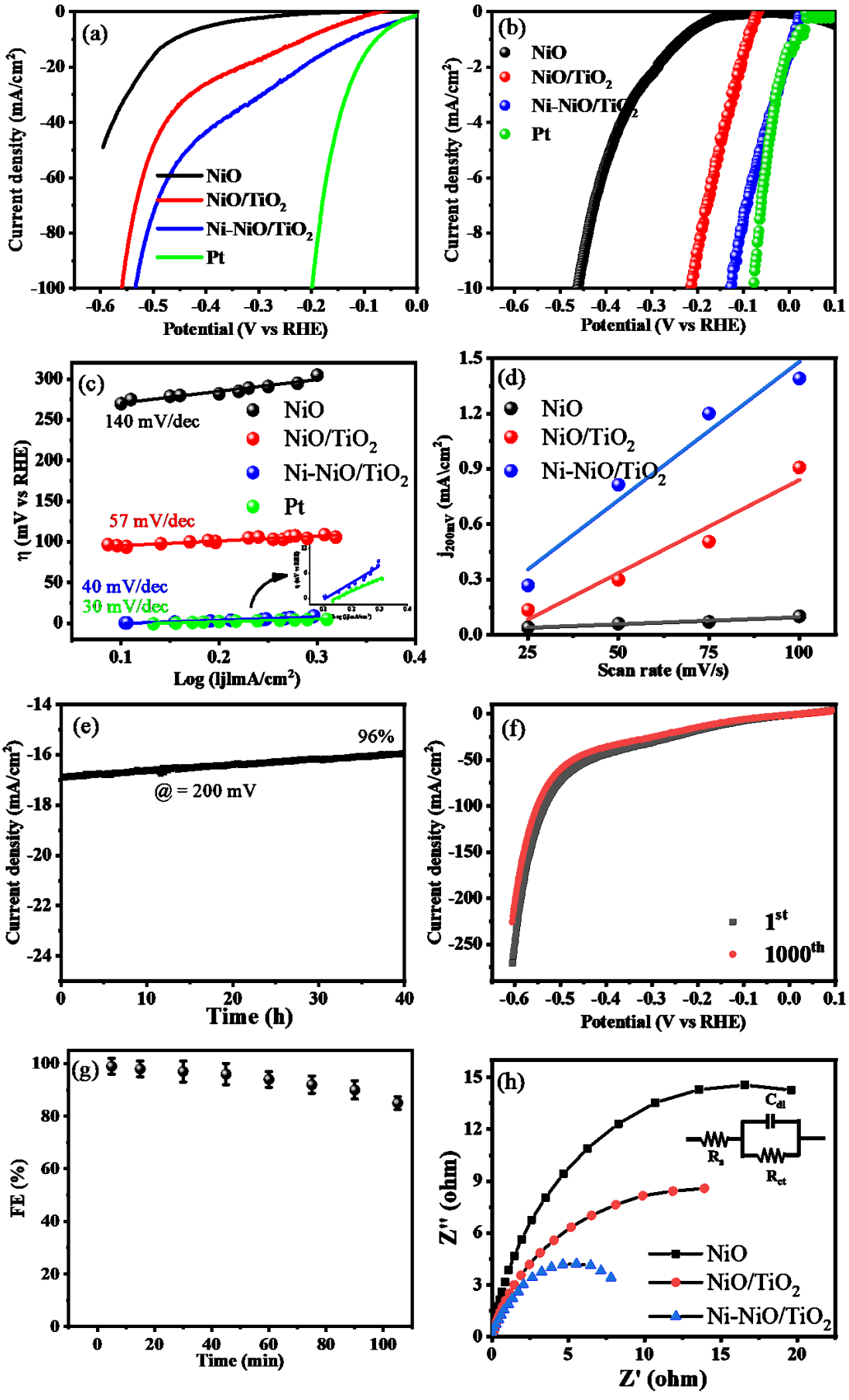
(a)
Current density (mA/cm²)
Potential (V vs RHE)
NiO
NiO/TiO2
Ni-NiO/TiO2
Pt
(b)
Current density (mA/cm²)
Potential (V vs RHE)
NiO
NiO/TiO2
Ni-NiO/TiO2
Pt
(c)
η (mV vs RHE)
Log (ljlmA/cm²)
140 mV/dec
57 mV/dec
40 mV/dec
30 mV/dec
NiO
NiO/TiO2
Ni-NiO/TiO2
Pt
(d)
j200mV (mA\cm²)
Scan rate (mV/s)
NiO
NiO/TiO2
Ni-NiO/TiO2
(e)
Current density (mA/cm²)
Time (h)
96%
@ = 200 mV
(f)
Current density (mA/cm²)
Potential (V vs RHE)
1st
1000th
(g)
FE (%)
Time (min)
(h)
Z'' (ohm)
Z' (ohm)
Cdl
Rs
Rct
NiO
NiO/TiO2
Ni-NiO/TiO2

Figure 4: Electrochemical Characterization of prepared catalysts, (a) Linear sweep voltammetry (LSV) curves depicting the performance of NiO, NiO/TiO_2, Ni-NiO/TiO_2, and Pt catayst for the hydrogen evolution reaction (HER) at 5 mV/s in 0.5 M H_2SO_4 electrolyte solution. (b) LSV curves at 10 mA/cm^2 comparing the tested catalysts with commercial Pt at 5 mV/s in 0.5 M H_2SO_4. (c) Tafel plots showcasing the electrocatalytic activity of the synthesized catalysts. The inset provides a magnified view of Ni-NiO/TiO2 and Pt. (d) Estimation of double-layer capacitance (C_{dl}) through the variation of current density ($\Delta j=(j_a-j_c)/2$) at 200 mV vs. RHE. (e) Chronoamperometry test of Ni-NiO/TiO_2 at 200 mV. (f) LSV curves before and after 5000 CV cycles with the Ni-NiO/TiO_2 electrode at 5 mV/s in 0.5 M H_2SO_4. (g) Faradic efficiency (FE) of Ni-NiO/TiO_2 at 300 mV vs. RHE for HER in 0.5 M H_2SO_4 saturated with Ar for 30 min before the experiment. The concentration of evolved H_2 was quantified every 15 min. (h) Electrochemical impedance spectroscopy (EIS) Nyquist plots in the frequency range of 0.1 Hz to 1 MHz with the equivalent circuit described in the inset.

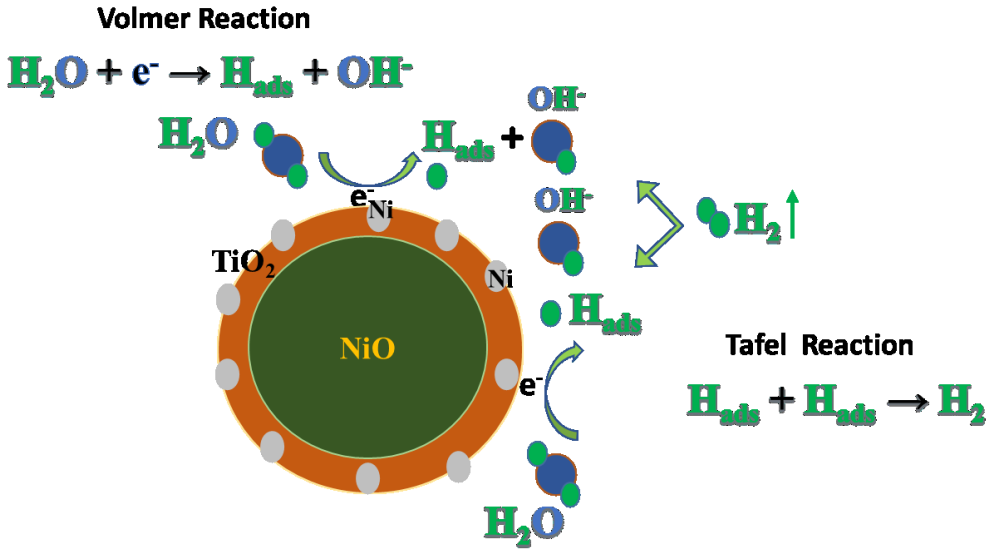

Figure 5: Mechanism of HER on the surface of Ni-NiO/TiO_2 core/Shell.

Table 2: Electrochemical data summary of the prepared catalysts for the HER

NFs	η_{10}, mv	η_{onset}, mv	TS_{HER}, mv/dec	C_{dl}, µF/cm^2	ECSA (cm^2)	j_0, mA.cm^{-2}	R_s, Ω	R_{ct}, Ω

NiO	455	274	140	7.6	0.19	2.01	0.045	39
NiO/TiO_2	205	160	56	101	2.54	2.64	0.040	27
$Ni\text{-}NiO/TiO_2$	125	88	40	190	4.75	2.97	0.030	11

Conclusion

This investigation pioneers a cost-efficient and streamlined methodology for the synthesis of core-shell structured electrocatalysts, namely NiO, NiO/TiO_2, and $Ni\text{-}NiO/TiO_2$, using a sol-gel approach, marking a breakthrough in electrocatalysis for hydrogen generation. Among these, the $Ni\text{-}NiO/TiO_2$ electrocatalyst emerges as a frontrunner, demonstrating an onset potential of merely ~88 mV, a Tafel slope of 40 mV/dec, and an exchange current density of 2.97 mA/cm². These figures highlight the system's efficiency and position it as a viable alternative to noble metal catalysts, steering the field towards sustainable energy innovations. The experimental narrative uncovered that integrating Ni into NiO/TiO_2 heterostructures significantly enhances the nanocore's electrochemical attributes. This enhancement is quantified by the superior electronic conduction and HER kinetics, where the $Ni\text{-}NiO/TiO_2$ configuration necessitates a notably reduced overpotential of 125 mV to achieve a current density of 10 mA/cm².

Furthermore, its endurance is showcased by maintaining structural and functional integrity across 1000 cycles of cyclic voltammetry (CV), a testament to its robustness surpassing conventional Pt catalysts. In-depth characterization via Rietveld refinement and SEM and TEM analyses provided pivotal insights into the electrocatalysts' crystallography, morphology, and composition. For instance, the Rietveld analysis confirmed the crystallite size reduction in the NiO phase when amalgamated with TiO_2, substantiating the SEM observations. The $Ni\text{-}NiO/TiO_2$ sample's lattice parameter reduction post-argon atmosphere calcination further corroborates the effective segregation of Ni, enhancing the material's electrocatalytic properties. In summary, this study not only underscores the $Ni\text{-}NiO/TiO_2$ electrocatalysts' exceptional performance in HER, evidenced by minimal onset potentials (~88 mV) and significant durability (sustained performance over 1000 CV cycles) but also highlights its potential in revolutionizing renewable hydrogen production. With a Faradaic efficiency of approximately 98% and superior performance metrics, the $Ni\text{-}NiO/TiO_2$ electrocatalyst stands as a monumental stride towards actualizing efficient, sustainable, and noble metal-free alternatives for energy conversion technologies.

Funding: The authors extend their appreciation to the Deanship of Scientific Research at Shaqra University for funding this research work.

Acknowledgements: The authors extend their appreciation to the Deanship of Scientific Research at Shaqra University for funding this research work.

References

[1] L. Wu *et al.*, "Catalytic activity of Ni–Cr–Fe–Mo porous materials for hydrogen evolution reaction in alkaline media," *Int. J. Hydrogen Energy*, vol. 69, pp. 1137–1148, 2024.

[2] M. K. Singla, P. Nijhawan, and A. S. Oberoi, "Hydrogen fuel and fuel cell technology for cleaner future: a review," *Environ. Sci. Pollut. Res.*, vol. 28, pp. 15607–15626, 2021.

[3] S. Dunn, "Hydrogen futures: toward a sustainable energy system," *Int. J. Hydrogen Energy*, vol. 27, no. 3, pp. 235–264, 2002.

[4] U. Y. Qazi, "Future of hydrogen as an alternative fuel for next-generation industrial applications; challenges and expected opportunities," *Energies*, vol. 15, no. 13, p. 4741, 2022.

[5] Y. Yu, S. J. Lee, J. Theerthagiri, Y. Lee, and M. Y. Choi, "Architecting the AuPt alloys for hydrazine oxidation as an anolyte in fuel cell: Comparative analysis of hydrazine splitting and water splitting for energy-saving H2 generation," *Appl. Catal. B Environ.*, vol. 316, p. 121603, 2022.

[6] S. Wang, A. Lu, and C.-J. Zhong, "Hydrogen production from water electrolysis: role of catalysts," *Nano Converg.*, vol. 8, pp. 1–23, 2021.

[7] F. Liu *et al.*, "Rational design of better hydrogen evolution electrocatalysts for water splitting: a review," *Adv. Sci.*, vol. 9, no. 18, p. 2200307, 2022.

[8] Y. Oh, J. Theerthagiri, M. L. Aruna Kumari, A. Min, C. J. Moon, and M. Y. Choi, "Electrokinetic-mechanism of water and furfural oxidation on pulsed laser-interlaced Cu2O and CoO on nickel foam," *J. Energy Chem.*, vol. 91, pp. 145–154, 2024.

[9] P. Purnami, W. Satrio Nugroho, Y. K. Sofi'i, and I. N. G. Wardana, "The impact of sodium lauryl sulfate on hydrogen evolution reaction in water electrolysis," *Int. J. Hydrogen Energy*, vol. 79, pp. 1395–1405, 2024.

[10] X. Liu *et al.*, "Adjusting surface electron density of heterostructured NiCo LDH/MXene/NF material to improve its electrocatalytic performance in hydrogen evolution reaction," *Int. J. Hydrogen Energy*, vol. 67, pp. 192–199, 2024.

[11] H. Gunaseelan, A. V Munde, R. Patel, and B. R. Sathe, "Metal-organic framework derived carbon-based electrocatalysis for hydrogen evolution reactions: A review," *Mater. Today Sustain.*, vol. 22, p. 100371, 2023.

[12] J. Li, Y. Xu, C. Wang, Z. Wu, Y. Shiraishi, and Y. Du, "Interfacial Engineering of Platinum Group Metals Electrocatalysts for Advanced Electrocatalysis," *Surfaces and Interfaces*, p. 103360, 2023.

[13] O. A. Petrii, "Pt–Ru electrocatalysts for fuel cells: a representative review," *J. Solid State Electrochem.*, vol. 12, pp. 609–642, 2008.

[14] S. Sarkar and S. C. Peter, "An overview on Pd-based electrocatalysts for the hydrogen

evolution reaction," *Inorg. Chem. Front.*, vol. 5, no. 9, pp. 2060–2080, 2018.
[15] Y. Attia and M. Samer, "Metal clusters: New era of hydrogen production," *Renew. Sustain. Energy Rev.*, vol. 79, pp. 878–892, 2017.
[16] S. Naik Shreyanka, J. Theerthagiri, S. J. Lee, Y. Yu, and M. Y. Choi, "Multiscale design of 3D metal–organic frameworks (M−BTC, M: Cu, Co, Ni) via PLAL enabling bifunctional electrocatalysts for robust overall water splitting," *Chem. Eng. J.*, vol. 446, p. 137045, 2022.
[17] R. A. Senthil *et al.*, "A facile one-pot synthesis of microspherical-shaped CoS2/CNT composite as Pt-free electrocatalyst for efficient hydrogen evolution reaction," *Int. J. Hydrogen Energy*, vol. 44, no. 31, pp. 16537–16547, 2019.
[18] S. Barua, A. Balčiūnaitė, D. Upskuvienė, J. Vaičiūnienė, L. Tamašauskaitė-Tamašiūnaitė, and E. Norkus, "3D Nickel–Manganese bimetallic electrocatalysts for an enhanced hydrogen evolution reaction performance in simulated seawater/alkaline natural seawater," *Int. J. Hydrogen Energy*, vol. 79, pp. 1490–1500, 2024.
[19] H. H. El-Maghrabi, A. A. Nada, S. Roualdes, and M. F. Bekheet, "Design of Ni/NiO–TiO2 /rGO nanocomposites on carbon cloth conductors via PECVD for electrocatalytic water splitting," *Int. J. Hydrogen Energy*, vol. 45, no. 56, pp. 32000–32011, 2020.
[20] W. Tan, X. Liu, W. Liu, H. He, and Y. Yang, "Galvanostatic electrodeposition of a self-supported Ni–Se–Lu/NF electrocatalyst for efficient alkaline hydrogen evolution reaction," *Int. J. Hydrogen Energy*, vol. 80, pp. 270–279, 2024.
[21] X. Zou *et al.*, "Phase-controlled synthesis of starch-derived Mo2C–MoC/C heterostructure catalyst for electrocatalytic hydrogen evolution reaction," *Int. J. Hydrogen Energy*, vol. 79, pp. 525–536, 2024.
[22] Y. Hao *et al.*, "Heterojunction catalysts of ultra-thin carbon layer activated Platinum nanoparticles for bifunctional pH-universal hydrogen evolution reaction and oxygen reduction reaction," *Int. J. Hydrogen Energy*, vol. 71, pp. 1242–1254, 2024.
[23] J. Chang *et al.*, "Enhanced electrocatalytic efficiencies for water electrolysis and para-nitrophenol hydrogenation by self-supported nickel cobalt phosphide-nickel iron layered double hydroxide pn junction," *J. Colloid Interface Sci.*, vol. 653, pp. 1063–1074, 2024.
[24] K. He *et al.*, "Utilizing the Space-Charge Region of the FeNi-LDH/CoP P-n Junction to Promote Performance in Oxygen Evolution Electrocatalysis," *Angew. Chemie Int. Ed.*, vol. 58, no. 34, pp. 11903–11909, 2019.
[25] H. Park, N. Son, B. H. Park, S. W. Joo, and M. Kang, "Visible light-induced stable HER performance using duality of ultrafine Pt NPs in a Z-scheme pn junction Fe2O3@ Pt@ FeS catalyst," *Appl. Surf. Sci.*, vol. 541, p. 148347, 2021.
[26] H. Zhao *et al.*, "np Heterojunction of TiO2-NiO core-shell structure for efficient hydrogen generation and lignin photoreforming," *J. Colloid Interface Sci.*, vol. 585, pp. 694–704, 2021.
[27] L. Wu, L. Ji, Y. Xiao, Q. Zhang, and Z. He, "Self-standing Ni–Cu–Ti/NCNTs electrocatalyst with porous structure for hydrogen evolution reaction," *Int. J. Hydrogen Energy*, vol. 64, pp. 819–829, 2024.
[28] G.-J. Sun, H. Kheel, S. Choi, S. K. Hyun, and C. Lee, "Prominent gas sensing performance of TiO2-core/NiO-shell nanorod sensors," *J. Nanosci. Nanotechnol.*, vol. 17, no. 6, pp. 4099–4102, 2017.
[29] J. Yang, L. Cheng, L. Wan, J. Yan, R. Chen, and H. Ni, "Fabrication of sandwich structured C/NiO/TiO2 nanotube arrays for enhanced electrocatalytic activity towards

hydrogen evolution," *Electrochem. commun.*, vol. 97, pp. 68–72, 2018.
[30] G. Bo *et al.*, "Preparation and electrochromic performance of NiO/TiO2 nanorod composite film," *J. Alloys Compd.*, vol. 728, pp. 878–886, 2017.
[31] C. Castañeda *et al.*, "Efficient NiO/F–TiO2 nanocomposites for 4-chlorophenol photodegradation," *Chemosphere*, vol. 315, p. 137606, 2023.
[32] C. Yu *et al.*, "NiO nanoparticles dotted TiO2 nanosheets assembled nanotubes PN heterojunctions for efficient interface charge separation and photocatalytic hydrogen evolution," *Appl. Surf. Sci.*, vol. 568, p. 150981, 2021.
[33] J. Pan *et al.*, "The photocatalytic hydrogen evolution and photoreduction CO2 selective enhancement of Co3O4/Ti3+-TiO2/NiO hollow core-shell dual pn junction," *J. Clean. Prod.*, vol. 380, p. 135037, 2022.
[34] J. Chen, M. Wang, J. Han, and R. Guo, "TiO2 nanosheet/NiO nanorod hierarchical nanostructures: p–n heterojunctions towards efficient photocatalysis," *J. Colloid Interface Sci.*, vol. 562, pp. 313–321, 2020.
[35] J. Yu, W. Wang, and B. Cheng, "Synthesis and enhanced photocatalytic activity of a hierarchical porous flowerlike p–n junction NiO/TiO2 photocatalyst," *Chem. Asian J.*, vol. 5, no. 12, pp. 2499–2506, 2010.
[36] A. Al-Kahlout, S. Heusing, and M. A. Aegerter, "Electrochromism of NiO-TiO 2 sol gel layers," *J. sol-gel Sci. Technol.*, vol. 39, pp. 195–206, 2006.
[37] M. Sabzi and S. H. M. Anijdan, "Microstructural analysis and optical properties evaluation of sol-gel heterostructured NiO-TiO2 film used for solar panels," *Ceram. Int.*, vol. 45, no. 3, pp. 3250–3255, 2019.
[38] R. Rameshbabu, N. Kumar, G. Pecchi, E. J. Delgado, C. Karthikeyan, and R. V Mangalaraja, "Ultrasound-assisted synthesis of rGO supported NiO-TiO2 nanocomposite: An efficient superior sonophotocatalyst under diffused sunlight," *J. Environ. Chem. Eng.*, vol. 10, no. 3, p. 107701, 2022.
[39] Z. Wu, Y. Wang, L. Sun, Y. Mao, M. Wang, and C. Lin, "An ultrasound-assisted deposition of NiO nanoparticles on TiO 2 nanotube arrays for enhanced photocatalytic activity," *J. Mater. Chem. A*, vol. 2, no. 22, pp. 8223–8229, 2014.
[40] S. M. Mirhadi, N. H. Nemati, F. Tavangarian, and M. D. Joupari, "Fabrication of hierarchical meso/macroporous TiO2 scaffolds by evaporation-induced self-assembly technique for bone tissue engineering applications," *Mater. Charact.*, vol. 144, pp. 35–41, 2018.
[41] T. Sreethawong, Y. Suzuki, and S. Yoshikawa, "Photocatalytic evolution of hydrogen over mesoporous TiO2 supported NiO photocatalyst prepared by single-step sol–gel process with surfactant template," *Int. J. Hydrogen Energy*, vol. 30, no. 10, pp. 1053–1062, 2005.
[42] T. Sreethawong, S. Ngamsinlapasathian, and S. Yoshikawa, "Surfactant-aided sol–gel synthesis of mesoporous-assembled TiO2–NiO mixed oxide nanocrystals and their photocatalytic azo dye degradation activity," *Chem. Eng. J.*, vol. 192, pp. 292–300, 2012.
[43] M. Rajesh, K. Vengatesan, M. H. Aly, R. Sitharthan, S. S. Dhanabalan, and M. Karthikeyan, "Electrical and optical properties of sol–gel-deposited NiO films and corresponding response to annealing temperature," *Opt. Quantum Electron.*, vol. 55, no. 13, pp. 1–17, 2023.
[44] H. Drobná *et al.*, "Partially Reduced Ni-NiO-TiO2 Photocatalysts for Hydrogen Production from Methanol–Water Solution," *Catalysts*, vol. 13, no. 2, p. 293, 2023.

[45] Ş. TOYGUN, G. KÖNEÇOĞLU, and Y. KALPAKLI, "General principles of sol-gel," *Sigma J. Eng. Nat. Sci.*, vol. 31, no. 4, pp. 456–476, 2013.
[46] W. Li, A. Elzatahry, D. Aldhayan, and D. Zhao, "Core–shell structured titanium dioxide nanomaterials for solar energy utilization," *Chem. Soc. Rev.*, vol. 47, no. 22, pp. 8203–8237, 2018.
[47] Q. Zhang, I. Lee, J. B. Joo, F. Zaera, and Y. Yin, "Core–shell nanostructured catalysts," *Acc. Chem. Res.*, vol. 46, no. 8, pp. 1816–1824, 2013.
[48] J. Feng, H. Zhou, D. Chen, T. Bian, and A. Yuan, "Core-shell structured ZnCo/NC@ MoS2 electrocatalysts for tunable hydrogen evolution reaction," *Electrochim. Acta*, vol. 331, p. 135445, 2020.
[49] Z. Zhao, J. Ding, R. Zhu, and H. Pang, "The synthesis and electrochemical applications of core–shell MOFs and their derivatives," *J. Mater. Chem. A*, vol. 7, no. 26, pp. 15519–15540, 2019.
[50] H. Feng *et al.*, "Core-shell nanomaterials: Applications in energy storage and conversion," *Adv. Colloid Interface Sci.*, vol. 267, pp. 26–46, 2019.
[51] S. S. Kanmani and K. Ramachandran, "Synthesis and characterization of TiO2/ZnO core/shell nanomaterials for solar cell applications," *Renew. Energy*, vol. 43, pp. 149–156, 2012.
[52] L. M. M. Correia, M. L. Kuznetsov, and E. C. B. A. Alegria, "Core–Shell Catalysts for Conventional Oxidation of Alcohols: A Brief Review," *Catalysts*, vol. 13, no. 7, p. 1137, 2023.
[53] A. Chinnappan, J. Dongxiao, W. Jayathilaka, C. Baskar, X. Qin, and S. Ramakrishna, "Facile synthesis of electrospun C@ NiO/Ni nanofibers as an electrocatalyst for hydrogen evolution reaction," *Int. J. Hydrogen Energy*, vol. 43, no. 32, pp. 15217–15224, 2018.
[54] M. Wu *et al.*, "NiO and CrO3 double surface-decorate Ni nanofibers for hydrogen evolution reduction," *Mater. Lett.*, vol. 182, pp. 15–18, 2016.
[55] J. Bao *et al.*, "Ultrathin spinel-structured nanosheets rich in oxygen deficiencies for enhanced electrocatalytic water oxidation," *Angew. Chemie*, vol. 127, no. 25, pp. 7507–7512, 2015.
[56] H. H. El-Maghrabi *et al.*, "Coaxial nanofibers of nickel/gadolinium oxide/nickel oxide as highly effective electrocatalysts for hydrogen evolution reaction," *J. Colloid Interface Sci.*, vol. 587, pp. 457–466, 2021.
[57] J. Yu, Y. Hai, and B. Cheng, "Enhanced photocatalytic H2-production activity of TiO2 by Ni (OH) 2 cluster modification," *J. Phys. Chem. C*, vol. 115, no. 11, pp. 4953–4958, 2011.
[58] X. Yin, L. Yang, and Q. Gao, "Core–shell nanostructured electrocatalysts for water splitting," *Nanoscale*, vol. 12, no. 30, pp. 15944–15969, 2020.
[59] D. Göhl *et al.*, "Engineering stable electrocatalysts by synergistic stabilization between carbide cores and Pt shells," *Nat. Mater.*, vol. 19, no. 3, pp. 287–291, 2020.
[60] B. M. Tackett *et al.*, "Reducing iridium loading in oxygen evolution reaction electrocatalysts using core–shell particles with nitride cores," *ACS Catal.*, vol. 8, no. 3, pp. 2615–2621, 2018.
[61] Y. Yu *et al.*, "Reconciling of experimental and theoretical insights on the electroactive behavior of C/Ni nanoparticles with AuPt alloys for hydrogen evolution efficiency and Non-enzymatic sensor," *Chem. Eng. J.*, vol. 435, p. 134790, 2022.
[62] H. H. El-Maghrabi *et al.*, "Coaxial nanofibers of nickel/gadolinium oxide/nickel oxide as highly effective electrocatalysts for hydrogen evolution reaction," *J. Colloid Interface*

Sci., 2020.
[63] A. G. Gavriliuk *et al.*, "The first-order structural transition in NiO at high pressure," *Commun. Phys.*, vol. 6, no. 1, p. 23, 2023.
[64] X. Gao, J. Ashok, and S. Kawi, "A review on roles of pretreatment atmospheres for the preparation of efficient Ni-based catalysts," *Catal. Today*, vol. 397–399, pp. 581–591, 2022.
[65] C. Wu, S. Deng, H. Wang, Y. Sun, J. Liu, and H. Yan, "Preparation of Novel Three-Dimensional NiO/Ultrathin Derived Graphene Hybrid for Supercapacitor Applications," *ACS Appl. Mater. Interfaces*, vol. 6, no. 2, pp. 1106–1112, Jan. 2014.
[66] A. Barhoum *et al.*, "Atomic layer deposition of Pd nanoparticles on self-supported carbon-Ni/NiO-Pd nanofiber electrodes for electrochemical hydrogen and oxygen evolution reactions," *J. Colloid Interface Sci.*, vol. 569, pp. 286–297, 2020.
[67] M. Gong *et al.*, "Nanoscale nickel oxide/nickel heterostructures for active hydrogen evolution electrocatalysis," *Nat. Commun.*, vol. 5, no. 1, p. 4695, 2014.
[68] S. Hu, F. Li, Z. Fan, and J. Gui, "Improved photocatalytic hydrogen production property over Ni/NiO/N–TiO2−x heterojunction nanocomposite prepared by NH3 plasma treatment," *J. Power Sources*, vol. 250, pp. 30–39, 2014.
[69] A. A. Nada, M. F. Bekheet, R. Viter, P. Miele, S. Roualdes, and M. Bechelany, "BN/GdxTi(1-x)O(4-x)/2 nanofibers for enhanced photocatalytic hydrogen production under visible light," *Appl. Catal. B Environ.*, vol. 251, pp. 76–86, 2019.
[70] A. Barhoum *et al.*, "Simultaneous Hydrogen and Oxygen Evolution Reactions using Free-Standing Nitrogen-Doped-Carbon-Co/CoOx Nanofiber Electrodes Decorated with Palladium Nanoparticles," *J. Mater. Chem. A*, 2021.
[71] S. Oh, H. Kim, Y. Kwon, M. Kim, E. Cho, and H. Kwon, "Porous Co–P foam as an efficient bifunctional electrocatalyst for hydrogen and oxygen evolution reactions," *J. Mater. Chem. A*, vol. 4, no. 47, pp. 18272–18277, 2016.
[72] S. Lu *et al.*, "Trash to treasure: A novel chemical route to synthesis of NiO/C for hydrogen production," *Int. J. Hydrogen Energy*, vol. 44, no. 31, pp. 16144–16153, 2019.
[73] P. Sivasakthi, S. Premlatha, G. N. K. R. Bapu, and M. Chandrasekaran, "Pulse electrodeposited Ni-CeO2Gd doped nanocomposite on copper foam as an electrocatalysts for hydrogen evolution reaction," *Int. J. Hydrogen Energy*, vol. 42, no. 8, pp. 4741–4750, 2017.
[74] S. S. Narwade, S. M. Mali, R. V Digraskar, V. S. Sapner, and B. R. Sathe, "Ni/NiO@ rGO as an efficient bifunctional electrocatalyst for enhanced overall water splitting reactions," *Int. J. Hydrogen Energy*, vol. 44, no. 49, pp. 27001–27009, 2019.
[75] Q. Dong, C. Sun, Z. Dai, X. Zang, and X. Dong, "Free-Standing NiO@ C Nanobelt as an Efficient Catalyst for Water Splitting," *ChemCatChem*, vol. 8, no. 22, pp. 3484–3489, 2016.
[76] X. Yan, L. Tian, and X. Chen, "Crystalline/amorphous Ni/NiO core/shell nanosheets as highly active electrocatalysts for hydrogen evolution reaction," *J. Power Sources*, vol. 300, pp. 336–343, 2015.
[77] P. He *et al.*, "Effect of Gd2O3 on the hydrogen evolution property of nickel–cobalt coatings electrodeposited on titanium substrate," *J. Phys. Chem. Solids*, vol. 72, no. 11, pp. 1261–1264, 2011.
[78] M. Chu *et al.*, "Carbon coated nickel-nickel oxide composites as a highly efficient catalyst for hydrogen evolution reaction in acid medium," *Electrochim. Acta*, vol. 264, pp. 284–

291, 2018.
[79] J. Huang *et al.*, “Mo-doped one-dimensional needle-like Ni3S2 as bifunctional electrocatalyst for efficient alkaline hydrogen evolution and overall-water-splitting,” *ChemPhysMater*, vol. 3, no. 1, pp. 74–82, 2024.